arXiv:astro-ph/9809051v1 4 Sep 1998

Constraints on the Physical Parameters of TeV Blazars

Fabrizio Tavecchio and Laura Maraschi
Osservatorio Astronomico di Brera, via Brera 28, 20100 Milano, Italy

and

Gabriele Ghisellini
Osservatorio Astronomico di Brera-Merate, via Bianchi 46, 22055 (Lecco), Italy.

ABSTRACT

We consider the constraints that can be derived from the spectral shape and variability of TeV blazars on the homogeneous synchrotron self–Compton (SSC) model. Assuming that the relativistic electron spectrum is a broken power law, where the break energy is a free parameter, we write analytical formulae that allow to connect observable quantities to the physical parameters of the model.We give approximate analytic formulae also for the case of Compton scattering occurring in the Klein Nishina regime, which is particularly relevant for TeV blazars. In particular we find that even in the latter regime a power law component can be present at the highest energies. Further restrictions in the parameter space are set assuming that the break energy results from a balance between cooling and escape and that the soft photon lags measured in some sources derive from radiative cooling of high energy particles. The constraints can be summarized as allowed regions in the Doppler factor – magnetic field parameter space and are in principle sufficient to univocally determine the model parameters and their uncertainties.

We apply the method to three well studied sources Mkr 421, PKS 2155–304 and Mkr 501. For Mrk 421 the available data are sufficient to fully constrain the model. The additional restrictions are found to be consistent with the model parameters, supporting the proposed interpretation. In the case of PKS 2155–304, not yet detected in the TeV band, we estimate the peak frequency of the Compton component ($\simeq 40$ GeV) and the expected TeV flux. The derived physical parameters are similar for the two sources, with a relatively large value of the Doppler factor ($\delta \sim 25$) and a magnetic field of $B \simeq 0.2$ G. For Mrk 501 we consider both the historical low state and the flaring state observed in April 1997. In the first case consistency between the various assumptions is reached for $\delta \simeq 10$ and $B \simeq 0.3$ G. For the high state a similar value of the Doppler factor and a somewhat larger value of the magnetic field are indicated, while the

extremely large frequency of the observed synchrotron peak requires continuous injection/reacceleration of relativistic particles.

Subject headings: BL Lacertae objects: general–gamma rays: observations– gamma rays: theory– radiation mechanisms: non-thermal–X-rays: theory

1. Introduction

The discovery of intense gamma-ray emission from blazars had a strong impact on our understanding of relativistic jets. Independent evidence of relativistic beaming was provided by the condition that the source should be transparent to high energy gamma-rays (Mattox et al. 1993, von Montigny et al. 1995, Dondi & Ghisellini 1995). The gamma-ray fluxes and spectra, together with data at lower frequency allowed detailed estimates of the physical parameters of different models (Maraschi, Ghisellini and Celotti 1992; Blandford 1993; Sikora, Begelman and Rees 1994; Dermer and Schlickeiser 1993).

More recently the discovery of TeV emission from some objects (Mrk 421, Mrk 501 and 1ES 2344+514) and the detection of very fast variability at these high energies motivated new theoretical and observational studies (e.g. Celotti, Fabian and Rees 1998)

The objects detected at TeV energies have similar spectral energy distributions (SED) from radio to X-rays. They emit synchrotron radiation with power peaking in the X-ray band. For Mrk 421 and Mrk 501 the X-ray and TeV radiation vary in a correlated fashion (Macomb et al. 1995, Buckley et al. 1996, Catanese et al. 1997, Schubnell 1997) suggesting that the TeV emission derives from the same high energy electrons responsible for the synchrotron X-rays. For Mrk 421 the TeV flux has been observed to vary with a 20 min timescale (Gaidos et al. 1996), which strongly limits the size of the emitting region. Furthermore a lag has been measured between soft and medium energy X-ray photons. A lag of the same order between soft and medium X-ray photons has been measured also in PKS 2155-304, whose spectral energy distribution closely resembles that of Mrk 421 up to the X-ray range, but has not yet been observed at TeV energies due to its southern declination. The lags strongly suggest a radiative origin yielding a new important constraint on the physical parameters of the emitting region. For Mrk 501, similar in spectral shape to the previous two, an extraordinary flaring behaviour has been observed recently (Pian et al. 1998).

The simplest model proposed for TeV blazars involves a single zone and a single population of relativistic electrons emitting synchrotron radiation from radio to X-rays

and inverse Compton radiation from X-rays to gamma-rays. For this class of sources the seed photons for the inverse Compton process are likely to be the synchrotron photons themselves (SSC) (see e.g. Ghisellini & Maraschi 1996, Mastichiadis & Kirk 1997), although other models have also been considered (for a review see Sikora 1997). We will limit ourselves to the SSC model in the following.

Our scope is to provide general analytic expressions for all the constraints that can be envisaged within this simple model and discuss the consequent restrictions in the parameter space for the above mentioned sources individually and as a group. A similar approach was initiated by Ghisellini, Maraschi and Dondi (1996) (hereafter GMD), however it did not include all the conditions and was limited to regimes well below the Klein Nishina limit, while for TeV blazars the Klein Nishina corrections are important. Work along these lines has been developed by Dermer, Sturner and Schlickeiser (1997) and by Bednarek and Protheroe (1997). The latter authors chose to use precise formulas requiring however numerical computations, with loss of generality.

The paper is organized as follows. In section 2 we discuss the constraints that can be put on the homogeneous SSC model using all the available observations. In section 3 the relevant formulae are derived which link model parameters to observative quantities. The effects of the Klein Nishina limit are discussed in detail and revised analytic formulae are given valid also in the latter regime. In section 4 we apply our diagnostics to the case of three well known blazars and finally (Section 5) we discuss the results.

2. Model constraints

The homogeneous SSC model assumes that radiation is produced in a single zone of the jet (approximated here for simplicity as a sphere with radius R), relativistically moving at small angle θ to the observer's line of sight. Photons up to the X-ray range are produced by relativistic electrons through the synchrotron process and are subsequently inverse Compton scattered by the same electrons to energies in the γ-ray range. The observed radiation will be strongly affected by relativistic effects. The key parameter is the Doppler factor $\delta = [\Gamma(1 - \beta\cos\theta)]^{-1}$, where Γ is the bulk Lorentz factor and $\beta = v/c$.

The observed SED of TeV emitting blazars (in a νF_ν plot) is characterized by two broad peaks, the first approximately in the X-ray band, the second in the 100 GeV-1 TeV band . Below and above the peaks the spectrum is quite smooth and can be approximated with power-law profiles with indices α_1, α_2 respectively where $\alpha_1 < 1$ and $\alpha_2 > 1$ (see e.g. GMD). Note that within the present uncertainties the "left" side of both peaks can be

described by the same spectral index. Note also that the spectrum in the TeV range is poorly known and may be affected by intergalactic absorption (see e.g. Stecker and De Jager 1997 and reference therein). In figure (1) we show the observed SED of Mrk 421 at two different epochs (Macomb et al. 1995).

The observed spectral shape requires that the the relativistic electron spectrum steepens with increasing energy. We approximate this behaviour with a broken power law (GMD) with indices $n_1 < 3, n_2 > 3$, respectively below and above the "break"energy $\gamma_b m_e c^2$:

$$N(\gamma) = \begin{cases} K\gamma^{-n_1} & \text{if } \gamma < \gamma_b \\ K\gamma_b^{n_2-n_1}\gamma^{-n_2} & \text{if } \gamma > \gamma_b \end{cases} \quad (1)$$

With these approximations we can completely specify the model using 7 parameters: the magnetic field intensity B, R, δ, the slopes n_1 and n_2, the Lorentz factor of the electrons at the "break", γ_b, and the electron density parameter K. The peak synchrotron power is emitted by electrons with the break energy $E_b = \gamma_b mc^2$. The maximum energy γ_{max} attained by electrons as well as a possible lower limit γ_{min} are unimportant here provided that $\gamma_{max} \gg \gamma_b$ and $\gamma_{min} \leq 100$

Spectra computed with the above assumptions are compared with the Mkn 421 data in Fig. 1. The theoretical curves show that the double power-law approximation can reproduce reasonably well the shape of the observed SED.

The available data on the SED can be used to derive 6 "observable" quantities of particular relevance for the above model, namely the indices α_1 and α_2, the frequency of the synchrotron and inverse Compton peaks, ν_s and ν_c, and the peak luminosities $L_s(\nu_s)$ and $L_c(\nu_c)$. These quantities are rather uncertain being ideally the result of a fitting procedure on simultaneous multifrequency data, but in practice often inferred from observations obtained at different epochs and with incomplete frequency coverage. The best sampled spectral region is usually the optical to X-ray range, therefore α_1, α_2, ν_s and $L_s(\nu_s)$ are better determined than ν_c and $L_c(\nu_c)$. Fig. 1 can serve as an illustration of the uncertainties in the determination of the "observables" for Mrk 421, perhaps the object with the best overall data. We recall that the one-zone homogeneous model is selfabsorbed at radio frequencies and cannot explain the radio emission which implies further contributions from the outer regions of the jet.

It is important that, at least in principle, one can derive from the broad band spectral observations 6 quantities that have to be reproduced with the 7 parameter model. One more observable quantity is sufficient to close the system. This can be provided by the minimum timescale of variation, t_{var}, which can be directly connected to the source dimension, R, through the causality relation $R \leq ct_{var}\delta$. This relation gives only an upper limit on

the dimension of the source, but a small dimension implies a high Doppler factor if the transparency condition is taken into account (see below). In order not to force δ to be too large we will adopt limits to the radius of the emission region in the range $ct_{var}\delta$- $\frac{1}{3}ct_{var}\delta$. At this point the system is closed and any additional constraint that can be satisfied should be regarded as supporting the model. These are:

- the transparency of the source to γ-rays.

  The high energy photons may interact with the low energy ones producing pairs. The fact that we observe the TeV emission poses a strong limit to the optical depth of the source to photon photon interaction and therefore to the energy density of the soft radiation. From this limit one can obtain a lower limit on the value of the Doppler factor (see e.g. Dondi & Ghisellini 1995).

- the radiative interpretation of the time lags in the light curves at different frequencies.

  Recently, observations of Mrk 421 and PKS 2155-304 with ASCA (0.3-10 keV) have revealed that when pronounced flares occur, the soft photons lag the harder ones (Takahashi et al. 1996, Urry et al. 1997). The simplest way to explain the time lags in a homogeneous model is through the hypothesis that they are associated to the time necessary for freshly injected high energy electrons to cool. With this assumption the measured time lags determine the cooling time setting a well defined condition on the model.

- the consistency of the break energy of the electrons with the condition of balance between cooling and escape.

  In our discussion the electron energy distribution is not calculated self-consistently (for an example of this alternative approach see e.g. Inoue and Takahara 1996, Mastichiadis and Kirk 1997, Ghisellini et al. 1998). The two spectral indices and the break energy are determined from the observed spectra. Having determined at the same time the dimension of the emission region and the magnetic and radiative energy densities we can verify a posteriori whether the cooling time of the electrons at the break is of the order of the escape (expansion) time from the emission region. We will assume that consistency is achieved if the required escape/expansion velocity is in the range $c/3 - c$. We recall however that in the standard hypothesis of a power law injection and subsequent cooling and escape in a homogeneous region, a spectral change $\Delta\alpha = 0.5$ is expected, while in general for the sources discussed below the observed steepening is larger, suggesting a more complex situation.

  We approximate the cooling time as the minimum between the synchrotron and the Compton cooling times. In the B–δ parameter space the regions of validity of these

two approximations are separated by the line expressing equipartition between the magnetic and radiation energy density. In each of these regions a value of the cooling time defines only one line. Bednarek & Protheroe (1997) discuss a similar constraint on the cooling time of the electrons, but they incorrectly apply the condition to both the synchrotron and the Compton cooling times *simultaneously* obtaining two independent constraints.

Summarizing, the SSC homogeneous model needs 7 independent parameters: the spectral observations give 6 independent quantities, and the seventh observational information used to close the system is the minimum variability timescale. Other constraints are provided by the optical depth for γ-γ interaction, by the observed time lags between soft and hard X-ray photons and by the consistency of the value of γ_b. These last conditions are additional independent constraints: if verified, these constraints argue for the physical consistency of a homogeneous SSC model.

3. Relations between the model parameters and observables

In this section we derive the fundamental relations between the model parameters and the observable quantities discussed above. We chose to do this analytically at the cost of some inevitable approximation in order to maintain generality. Most of these formulae are also discussed in GMD and Dermer et al. (1997).

We assume that the two spectral indices can be determined directly from the data, independently of other quantities. The structure of the relations is then such that we can eliminate 3 of the remaining 5 parameters (i.e. γ_b, K and R) and express the constraints as allowed regions in the B-δ parameter space.

3.1. Peak frequencies

In the scheme that we consider the dominant synchrotron power is emitted by electrons at the break (those with Lorentz factor γ_b). Primed quantities refer to the blob frame so that the observed frequency is given by $\nu_s = \nu'_s\delta$. The photons at ν_s dominate the energy density of the target photons and the inverse Compton power in the Thomson limit will be dominated by photons at frequency $\nu_c = (4/3)\gamma_b^2\nu'_s\delta$, produced in the scattering between the electrons at the break and the photons with frequency ν'_s (see also GMD). Inverting the last equation one obtains:

$$\gamma_b = \left(\frac{3\nu_c}{4\nu_s}\right)^{1/2} \tag{2}$$

Therefore the ratio between the peak frequencies gives directly the value of γ_b.

The synchrotron frequency averaged over the spectral shape for an electron of Lorentz factor γ_b is:

$$\nu_s = 3.7 \cdot 10^6 \gamma_b^2 B \frac{\delta}{1+z} \tag{3}$$

using the value of γ_b given by eq. (2), gives:

$$B\delta = (1+z)\frac{\nu_s^2}{2.8 \cdot 10^6 \nu_c} \tag{4}$$

The last formula shows that for fixed ν_s and ν_c, B and δ are inversely proportional. We will see in the next section that in the KN limit this situation is reversed.

3.2. Peak luminosities

Another relation can be obtained from the ratio of the total luminosity of the synchrotron peak and the total luminosity of the self-Compton peak, which is directly related to the ratio between the radiation and the magnetic field energy densities inside the source (in the comoving frame):

$$\frac{L_c}{L_s} = \frac{U'_{syn}}{U'_B} \tag{5}$$

For our aims it is useful to express the total luminosity through the peak luminosity, which is more accessible to observations. A simple calculation shows that the total luminosities (L_s and L_c) and the peak luminosities [$L_s(\nu_s)$ and $L_c(\nu_c)$] are related by:

$$L_{s,c} = f(\alpha_1, \alpha_2)\nu_{s,c}L_{s,c}(\nu_{s,c}) \tag{6}$$

where $f(\alpha_1, \alpha_2)$ is given by

$$f(\alpha_1, \alpha_2) = \frac{1}{1-\alpha_1} + \frac{1}{\alpha_2 - 1} \tag{7}$$

Expressing U'_{syn} as:

$$U'_{syn} = \frac{L_s}{4\pi R^2 c \delta^4} \tag{8}$$

we can rewrite eq. (5) as:

$$\frac{L_c}{L_s} = \frac{\nu_c L_c(\nu_c)}{\nu_s L_s(\nu_s)} = \frac{2\nu_s L_s(\nu_s) f(\alpha_1, \alpha_2)}{R^2 c \delta^4 B^2} \tag{9}$$

If we express the source dimension R with the variability timescale

$$R \leq c t_{var} \delta (1+z)^{-1} \tag{10}$$

we can finally write:

$$B\delta^3 \geq (1+z) \left[\frac{2(\nu_s L_s(\nu_s))^2 f(\alpha_1, \alpha_2)}{c^3 t_{var}^2 \nu_c L_c(\nu_c)} \right]^{1/2} \tag{11}$$

This formula relates the magnetic field intensity and the Doppler factor to observable quantities. Eq. (11) is an inequality because of the use of the inequality eq. (10); taking $ct_{var}/3$ as a lower limit on the radius of the source, as discussed in Section 2, eq. (11) will be represented in the B, δ space by a strip of finite width. Thus the intersection of eq. (11) with eq. (4) allows to estimate B and δ.

4. The Klein Nishina regime

4.1. Spectral shape of the Inverse Compton emission

The adopted spectral shape for the electrons ensures that the synchrotron spectrum has a well defined peak (break) (as observed). Thus both, electrons and photons, have a low energy branch and a high energy branch (below and above the break). With the adopted approximations one can compute the inverse Compton spectrum as the sum of 4 separate integrals: $I_{1,1}, I_{1,2}$ and $I_{2,1}$, $I_{2,2}$, representing the contributions from electrons of the low

(1) and high (2) energy branches scattering photons of the low and high energy branches respectively. Full expressions are given in the Appendix. This subdivision is very useful in the discussion of the Klein Nishina limit.

The different contributions, computed using the well known δ-function approximation for the single electron emission and a step function for the energy dependence of the cross section, $\sigma = \sigma_T$ for $\gamma\nu' < 3/4$ and $\sigma = 0$ otherwise (see Coppi and Blandford 1990 for a critical discussion), are shown in Fig. 2. All the spectra are computed in the source frame for fixed values of $\nu'_s = 10^{15}$ Hz and varying γ_b from 10^3 to 10^6, that is for increasing importance of the KN limit.

Since the assumed particle spectra have no high energy cut offs, at high enough energy, the KN limit is always relevant and steepens the spectrum. The limiting frequency can be estimated considering that the largest contribution to the radiation energy density is due to photons of frequency ν'_s. Therefore the KN limit will set in at a frequency $\nu'_K \geq (mc^2/h)^2/\nu'_s$. This is seen in Fig. 2a and 2b, where three (12, 21, 22) of the four components in the total spectrum cut off at high energies, while the peak of the inverse Compton spectrum occurs as expected in the Thomson limit.

However the effect will be severe and affect both the value of the peak frequency and the bulk of the emitted power if ν_K is close to ν_C, that is if the KN regime sets in already for the scattering of electrons of energy γ_b with photons at the peak of the synchrotron emission. Therefore the condition for the KN regime to affect severely the luminosity and the peak frequency of the inverse Compton emission, requiring a revision of the formulae given in section 3 is:

$$\gamma_b \nu'_s \geq \frac{3}{4}\frac{mc^2}{h} \tag{12}$$

Using eq. (2) for γ_b to express the above condition with observed quantities, eq. (12) becomes a condition on δ:

$$\delta < \delta_{KN} = \left[\frac{\nu_c \nu_s}{(3/4)(mc^2/h)^2}\right]^{1/2} \tag{13}$$

Since eq. (2) (valid in the Thomson limit) gives the lowest possible value of γ_b, eq. (13) gives the limit above which the full KN regime sets in. However even for δ somewhat above the KN limit corrections are non negligible (see Section 4.2)

The contribution involving both electrons and photons on the high energy branches

($I_{2,2}$) is already strongly suppressed in Fig. 2b and disappears completely when the KN condition is met (Fig. 2c, 2d). The other contributions are reduced according to the availability of photons below the KN threshold. In Fig. 2c and 2d $I_{1,2}$ is negligible and the low energy side is dominated by by the $I_{1,1}$ branch.

It is interesting to note that for the assumed spectral shape the scattering of highest energy electrons with very low energy photons gives a significant power law contribution to the inverse Compton spectrum at the highest energies. The latter component is not important energetically (at the peak) however it provides a high energy tail which extends the range of the inverse Compton emission. The spectral index of the latter contribution can be easily derived from the expression for $I_{2,1}$ given in the Appendix and is $\alpha_{KN} = 2\alpha_2 - \alpha_1$. This component could explain the power law spectra measured in the TeV range for Mrk 421 and Mrk 501 (Zweerink et al. 1997).

4.2. Compton peak frequency and luminosity in the KN limit

In the KN regime both the expression of the Compton peak frequency and luminosity must be modified. As shown in Fig. 2c, 2d, with the assumed electron spectrum the peak frequency in the KN limit is determined by the scattering between all the electrons and photons with $\nu < \nu_s$. Maximizing the sum of $I_{1,1}$ and $I_{2,1}$ (see Appendix) leads to the following relation between ν_c and γ_b:

$$\nu_c = \nu'_c \frac{\delta}{1+z} \simeq \frac{mc^2}{h} \gamma_b g(\alpha_1, \alpha_2) \frac{\delta}{1+z} \tag{14}$$

where:

$$g(\alpha_1, \alpha_2) = \exp\left[\frac{1}{\alpha_1 - 1} + \frac{1}{2(\alpha_2 - \alpha_1)}\right] \tag{15}$$

is a factor smaller than one.

Substituting γ_b derived from eq. (14) in eq. (3) we obtain:

$$\frac{B}{\delta} = \frac{\nu_s}{\nu_c^2} \left(\frac{mc^2}{h}\right)^2 \frac{g(\alpha_1, \alpha_2)^2}{3.7 \cdot 10^6} \frac{1}{1+z} \tag{16}$$

which is the analogous of the eq. (4) for the KN regime. Note that in this equation B and δ are directly proportional.

Having obtained a revised expression of eq. (2) we can use the latter (eq. [14]) to

express (12) through observables. We therefore arrive at a revised version of the threshold for the KN regime:

$$\delta < \delta_{KN} = \left[\frac{\nu_c \nu_s}{(3/4)(mc^2/h)^2}\right]^{1/2} g(\alpha_1, \alpha_2)^{-1/2} \tag{17}$$

Since $g(\alpha_1, \alpha_2)$ is less than 1, eq. (17) is more stringent than eq. (13): therefore we find two *different* limits dividing the regions of applicability of the two treatments. Between this two limits there is a transition region, where both the approaches are approximations.

In the KN regime the power in the Compton peak is substantially diminished. equation (5) should be replaced by:

$$\frac{L_c}{L_s} = \frac{U'_{syn,avail}}{U'_B} \tag{18}$$

where $U'_{syn,avail}$ includes only photons below the KN limit for electrons with the break energy, that is with $\nu'_0 \leq mc^2/h\gamma_b$. We can write:

$$U'_{syn,avail} = \int_0^{3mc^2/4h\gamma_b} \epsilon'_{syn}(\nu'_0) d\nu'_0 \tag{19}$$

where $\epsilon'_{syn}(\nu'_0)$ is the energy density of the synchrotron radiation for a given frequency. A simple calculation shows that the integral is given by:

$$U'_{syn,avail} = U'_{syn} \left(\frac{3mc^2\delta}{4h\gamma_b\nu_s}\right)^{1-\alpha_1} \tag{20}$$

where the factor in parentheses represents the ratio between the available energy density and the total energy density. From the last relation we can obtain the following expression for the energy density ratio in the comoving frame in the KN regime:

$$\frac{U'_{syn}}{U'_B} = \frac{L_c}{L_s}\left[\frac{3}{4}\left(\frac{mc^2}{h}\right)^2 \frac{\delta^2}{\nu_s\nu_c}\frac{g(\alpha_1,\alpha_2)}{1+z}\right]^{\alpha_1-1} \tag{21}$$

Using the last formula and expressing the total luminosities through eq. (6) and the radius with eq. (10) we can finally obtain the analogous of eq. (11) for the KN limit:

$$B\delta^{2+\alpha_1} > (1+z)^{\alpha_1} \left[\frac{g(\alpha_1,\alpha_2)}{\nu_c\nu_s}\right]^{(1-\alpha_1)/2} \left[\frac{2(\nu_s L_s(\nu_s))^2 f(\alpha_1,\alpha_2)}{c^3 t_{var}^2 \nu_c L_c(\nu_c)}\right]^{1/2} \left(\frac{3mc^2}{4h}\right)^{1-\alpha_1} \tag{22}$$

5. Additional constraints on the model parameters

5.1. The pair production opacity

Another strong constraint is obtained from the condition of transparency of γ-rays to pair-production absorption. Following Dondi & Ghisellini (1995) we can write this condition in the form:

$$\delta > \left[\frac{\sigma_T}{5hc^2} d_L^2 (1+z)^{2\beta} \frac{F(\nu_0)}{t_{var}}\right]^{1/(4+2\beta)} \tag{23}$$

where $\nu_0 = 1.6 \cdot 10^{40}/\nu_\gamma$ is the frequency of target photons and β is the spectral index of the target photons (α_1 for $\nu_0 < \nu_s$ and α_2 for $\nu_0 > \nu_s$). The transparency condition does not depend on the specific emission mechanisms: therefore it provides a strong independent constraint on the minimum value of the Doppler factor in the SSC model.

5.2. Cooling time

The radiative cooling time for a synchrotron–self Compton emitting electron is given by:

$$t'_{cool} = \left[\frac{4}{3}\frac{\sigma_T c}{mc^2}\gamma(U'_B + U'_{syn,avail})\right]^{-1} \tag{24}$$

Clearly the cooling time is determined by the fastest of the two cooling processes that is synchrotron cooling for $U'_B > U'_{syn,avail}$ or inverse Compton cooling for $U'_B < U'_{syn,avail}$. Let us first consider for simplicity the Thomson regime. In the case in which the magnetic field energy density dominate we can approximate the cooling time as (after some manipulations):

$$t'_{cool} \simeq t'_{sync} = C_s B^{-3/2} \delta^{1/2} \nu^{-1/2} \tag{25}$$

while in the opposite case (using eq. [8] for the energy density and expressing γ with eq. [3]):

$$t'_{cool} \simeq t'_{comp} = C_c B^{1/2} \delta^{13/2} \nu^{-1/2} \tag{26}$$

where C_s and C_c are constants.

In the observer frame:

$$t_{sync} = C_s B^{-3/2} \delta^{-1/2} \nu_s^{-1/2};\ t_{comp} = C_c B^{1/2} \delta^{11/2} \nu_s^{-1/2} \tag{27}$$

The equipartition condition $U'_B = U'_{rad}$ divides the regions of validity of the two approximations in the $B - \delta$ plane. The Compton cooling approximation will be valid in the lower region (where $U'_B < U'_{sync}$), while the synchrotron cooling approximation will be valid in the upper region. In both cases a given value of t_{cool} defines an inverse relation between B and δ, that is lines with negative slopes, intersecting each other at the equipartition line (see Figures in the Application sections). Thus a condition on the cooling time corresponds to a minimum value of δ above which the condition is represented by a double valued function with two branches. Lower values of δ correspond to shorter cooling times.

5.3. Time lags

The measurement of time delays between variations in different energy bands provides an important restriction on the possible values of the physical parameters of the model. The most natural way to explain the lags in a homogeneous model is to interpret them as due to the cooling time of the emitting electrons (Takahashi et al. 1996, Urry et al. 1997). In this picture the quiescent emission is produced by the "stationary" population of electrons, while the flare is due to the injection of a monoenergetic population of high energy electrons: while these electrons cool their emission drifts to lower frequencies as observed. Adopting this hypothesis we can relate the observed time lags to the cooling time of the electrons and therefore to the physical parameter of the source. If the cooling is dominated by the synchrotron emission (i.e. $U'_B \geq U'_{syn}$, where U'_{syn} is $U'_{syn,avail}$ in the KN limit), we obtain the following relation (see also Takahashi et al. 1996):

$$B\delta^{1/3} = 300 \left(\frac{1+z}{\nu_{1,17}} \right)^{1/3} \left[\frac{1 - (\nu_1/\nu_0)^{1/2}}{\tau_{obs}} \right]^{2/3} G \tag{28}$$

where ν_0 and ν_1 are the X-ray frequencies ($\nu_0 > \nu_1$) and τ_{obs} is the measured lag (in seconds). In the Compton cooling dominated region (i.e. $U'_B \leq U'_{syn}$) we can write the equivalent relation:

$$B\delta^{11} = \frac{3.7 \cdot 10^{-8}}{1+z} \nu_{1,17} \left[\frac{2\nu_s L_s(\nu_s) f(\alpha_1, \alpha_2)}{c^3 t_{var}^2} \frac{\tau_{obs}}{1-(\nu_1/\nu_0)^{1/2}} \right]^2 \tag{29}$$

5.4. Cooling vs. escape

In our approach the value of γ_b enters as a free parameter in the model and is determined from the observations. However in more sophisticated models γ_b could be determined selfconsistently by the equilibrium between injection, cooling and escape of electrons from the source. Here we include a posteriori the condition that the cooling time at γ_b is equal to the escape time. The latter constraint can be written as:

$$\frac{R}{\beta_{esc} c} = \left[\frac{4}{3} \frac{\sigma_T c}{mc^2} \gamma_b (U'_B + U'_{syn,avail}) \right]^{-1} = \frac{5 \cdot 10^8}{\gamma_b B^2 (1 + U'_{syn,avail}/U'_B)} \tag{30}$$

where β_{esc} is the electron escape velocity in unit of c and U'_B and $U'_{syn,avail}$ are, respectively, the magnetic field energy density and the radiation energy density.
If cooling is dominated by the synchrotron process, expressing (30) in terms of the observational quantities ν_s and ν_c gives:

$$B\delta^{1/2} > \left[\frac{5 \cdot 10^8 (\nu_s/\nu_c)^{1/2} (1+z)}{t_{var}} \right]^{1/2} \beta_{esc}^{1/2} \tag{31}$$

for the Thomson limit and:

$$B > \left[\frac{5 \cdot 10^8 g(\alpha_1, \alpha_2)}{t_{var}} \frac{mc^2}{h} \frac{1}{\nu_c} \right]^{1/2} \beta_{esc}^{1/2} \tag{32}$$

for the KN limit.

Even when Compton cooling is less important than synchrotron cooling, if it occurs in the KN regime, the value of γ_b must be taken from eq. (14) instead of eq. (2), which causes the difference between (31) and (32).

In the Compton-cooling dominated region the equations are:

$$B\delta^{11} > 5.2 \cdot 10^{-14} \left[\frac{\nu_s L_s(\nu_s) f(\alpha_1,\alpha_2)}{c^3}\right]^{2.1} \left[\beta_{esc}(\nu_s/\nu_c)^{1/2}(1+z)\right]^{-8/5} t_{var}^{-13/5} \qquad (33)$$

for the Thomson regime and:

$$B\delta^{6/(1-\alpha_1)} = \xi(\alpha_1,\alpha_2) \left[\frac{\nu_s L_s(\nu_s) f(\alpha_1,\alpha_2)}{t_{var}\beta_{esc}}\right]^{1/(1-\alpha_1)} [\nu_c(1+z)]^{(3\alpha_1-2)/(1-\alpha_1)} \qquad (34)$$

[$\xi(\alpha_1,\alpha_2)$ is a constant given in the Appendix] for the KN regime.

The electron escape time is not a well known parameter and depends on the transport processes in the emitting region: in the applications we check the consistency of the observed value of γ_b for values of β_{esc} in the range $1 - 1/3$.

6. Applications

In the previous section we have shown that the constraints considered lead to equations that can be expressed in terms of two parameters: the magnetic field and the Doppler factor. Each constraint then corresponds to an allowed region or to a line in the Log B - Log δ plane. Three equations do not apper explicitly: one determines γ_b from the peak frequencies, the second determines the radius from the variability timescale, the third the normalization constant of the electron spectrum from the observed synchrotron luminosity. We examine here what consequences can be derived comparing the constraints available for the three brightest and best observed BL Lacs with synchrotron peaks near or within the X-ray band.

6.1. Mrk 421

We start from the following values for the observable quantities, derived from the simultaneous observations of Macomb et al. (1995) (the corresponding data are shown in Fig. 1) : $\nu_s = 3 \cdot 10^{16}$ Hz, $\nu_c = 6.5 \cdot 10^{25}$ Hz, $\alpha_1 = 0.5$, $\alpha_2 = 1.75$ $\nu_s L_s(\nu_s) = 4.7 \cdot 10^{44}$ erg s^{-1} and $\nu_c L_c(\nu_c) = 6.5 \cdot 10^{44}$ erg s^{-1} (see Table 1). These refer to the low state (for the high state we find similar results for the values of B and δ). The TeV observations show extremely short variability timescales (Gaidos et al. 1996 report a flare with $t_{var} \simeq 20$ min), while in the X-ray band variability timescales of several hours are observed (see Takahashi et al. 1996): in Fig. (3) we have used $t_{var} \simeq 1$ h. For Mrk 421 the soft photon lag within

the ASCA band was measured by Takahashi et al (1996) yielding $\tau_{obs} = 3200$ s between $E_1 = 1$ keV and $E_2 = 5$ keV.

In Fig. (3) we show the parameter space for Mrk 421. The transparency condition (23) calculated for photons with $\nu = 10^{26}$ Hz yields a lower limit $\delta > 15$ represented by the vertical line. The KN condition [eq. (13)] yields an upper limit $\delta < 14$, while the more stringent version [eq. (17)] yields $\delta < 31$. For $14 < \delta < 31$ we are therefore in an intermediate region where both limits are inaccurate. We chose to use the Thompson limit here since the resulting value of δ will be 25, close to the upper end. We recall however that even if the Thomson limit is adequate for the peak of the Compton component, KN effects cannot be neglected in the computation of spectra at higher energies (see Fig. 1, Fig. 2a).

The observed ratio between the two peak frequencies [eq. (4)] imposes an inverse proportionality relation between B and δ. This is shown as a shaded area allowing for a factor 3 uncertainty in the actual value of the Compton peak frequency.

The ratio of the peak luminosities (11) yields a steeper relation between B and δ, $B \propto \delta^{-3}$. Again it is represented by a shaded area to allow for uncertainties in the observational input data.

The intersection between the two regions above defines the allowed region, where the actual values of the parameters should fall. This region could shrink if the observational data improve, but given the present gap between the energy ranges of EGRET and the ground based Cherenkov telescopes it is unlikely that it could be substantially reduced.

The time lag constraint has a shallow dependence on δ ($B \propto \delta^{-1/3}$) and is well defined observationally. Therefore it is represented as single thick line (labelled l) in Fig. 3. It is extremely interesting that this line, which is completely independent of the spectral constraints, is consistent with the parameter region allowed by those constraints. It is also interesting that the region defined by the condition that the break energy of the electrons is determined by a balance between cooling and escape eq. (31) (region C) encompasses the lag constraint in the relevant parameter interval.

We conclude that for Mrk 421 the spectral constraints are consistent both with the radiative interpretation of the soft photon lag and with the break energy as due to cooling. These are persuasive arguments in support of the simple general model. The estimated parameter values are $B \simeq 0.25$ and $\delta \simeq 25$ (see Table 2)

Note that the value of δ is rather high compared to other estimates (Ghisellini et al. 1998) but similar to that found from direct model fits by Mastichiadis & Kirk (1997) and Ghisellini & Maraschi (1996).

6.2. PKS 2155-304

This BL Lac object has been studied for a long time with numerous multifrequency campaigns (Urry et al. 1997; Edelson et al. 1995). It has been detected as a γ-ray source by EGRET on one occasion (Vestrand et al. 1995) and more recently in a flaring state (IAU Circ. 6774). No simultaneous X-ray and gamma-ray observations are available yet. It has not been detected in the TeV band. This may however be due to its southern declination, since in the southern hemisphere Cherenkov telescopes have started observations only recently.

The parameters of the synchrotron component are inferred from the spectrum measured during the 1994 multifrequency campaign ($\nu_s = 10^{16}$ Hz and $\nu_s L(\nu_s) = 1.5 \cdot 10^{46}$ erg s^{-1}, Urry et al. 1997). Comparison with previous observations (see Sambruna et al. 1994) shows that during these observations PKS 2155-304 was in an intermediate state, a factor 2 less luminous than the brightest state recorded by EXOSAT.

The gamma-ray spectrum measured with EGRET is hard, implying that the Compton peak is beyond the EGRET range. However the absence of TeV observations does not allow to determine the position of the peak. We will therefore use the other constraints to estimate the peak frequency of the Compton emission and the associated TeV luminosity, assuming that all of them should be satisfied as is the case for Mkn 421.

In Fig. (4) we show the parameter obtained for $\nu_c = 10^{25}$ Hz and for an "observed" luminosity of $\nu_c L(\nu_c) = 1.5 \cdot 10^{46}$ erg s^{-1} extrapolated from the GeV range. We assume a minumum variability time of $t_{var} = 2 \cdot 10^4$ s and a delay of $\tau_{obs} \simeq 5 \cdot 10^3$s between the variations observed in the 0.75 keV and 6 keV energy bands (Urry et al. 1997). The vertical line representing the transparency condition is plotted for photons with frequency $\nu \simeq 10^{25}$ Hz for consistency with the following estimates of the TeV flux. Note, however, that the lower limit on the Doppler factor given by the transparency condition would be weaker in the absence of TeV emission.

In this case, the largest uncertainty is on the position of the Compton peak, while the frequency of the synchrotron peak is reasonably well known. We therefore plot the uncertainty band for fixed ν_s and for ν_c ranging from $2.5 \cdot 10^{24}$ Hz to $2.5 \cdot 10^{25}$ Hz. For these values of the peak frequencies the KN limit yields $\delta_{KN} < 3$, smaller than the transparency limit: we can make use of the Thomson formulation.

We find that all the constraints are satisfied for values of B and δ very similar to those found in Mrk 421 ($B \simeq 0.25$ and $\delta \simeq 25$); the cooling-escape consistency for γ_b is satisfied also in this case.

We can estimate the value of the TeV flux of PKS 2155-304 with the hypothesis that beyond the break the spectral indices of Mrk 421 and PKS 2155-304 are similar. From the spectrum of Mrk 421 we can obtain the value $\alpha_{TeV} \simeq 2.2$; from the inferred value of the γ peak flux of PKS 2155-304 we can evaluate the TeV flux as:

$$F_{TeV} = F(\nu_c) \left(\frac{\nu_{TeV}}{\nu_c} \right)^{-\alpha_{TeV}} \tag{35}$$

that gives an integrated flux $F(> 1TeV) \simeq 10^{-11}$ ph s^{-1} cm^{-2}, about 25% that of Mrk 421 in the in the non-flaring state. Hence we expect that a detection of PKS 2155-304 should be possible but requires sufficient sensitivity, due to the low flux. TeV observations of PKS 2155-304 would be extremely important also because they may reveal or constrain absorption of high energy photons by the intergalactic IR background (Stecker and De Jager 1997), better than in the case of Mrk 421 because of the larger distance.

6.3. Mrk 501

The BL Lac object Mrk 501 (z=0.034) underwent a dramatic TeV and X-ray outburst in April 1997 (see e.g. Pian et al. 1998, Catanese et al. 1997). Previous observations showed a spectral distribution very similar to Mrk 421, with a synchrotron peak in the soft X-ray region; in contrast, during the April observation the peak was found at about 100 keV, a shift in energy of at least a factor 100. The broad band spectral shape leads to interpret the hard X-ray emission as synchrotron radiation and the flare as due to injection of electrons with very high energy (Pian et al. 1998).

In Fig. (5) we show the parameter space for Mrk 501 in the quiescent state. In this state we can apply the relation for the Thomson case, given that the value of δ required by the transparency condition is higher than δ_{KN}. We have used the following values for the observable quantities: $\nu_s = 10^{16}$ Hz, $\nu_c = 10^{25}$ Hz, $\nu_s L_s(\nu_s) = 10^{44}$ erg/s, $\nu_c L_c(\nu_c) = 5 \cdot 10^{43}$ erg/s, $t_{var} \simeq 10$ h, $\alpha_1 = 0.5$ and $\alpha_2 = 1.75$.
For the quiescent state we have large uncertainties on the position of the Compton peak: the boundaries of region A refer to values of $\nu_c \simeq 3 \cdot 10^{24}$ Hz (upper line) to $\nu_c \simeq 3 \cdot 10^{25}$ Hz.

Since a measurement of a time lag between variations in different frequencies is lacking the associated constraint cannot be used.

The longer variability timescales and the lower luminosity with respect to the two previous sources allow in this case a value of δ around 10, lower than those inferred in Mrk 421 and PKS 2155-304, as can be seen from Fig. (5), while the value found for the magnetic field intensity, $B \simeq 0.3$ is similar.

For the high state we must use the formulation in the KN limit: in fact the Thomson condition (13) yields a value of $\delta \simeq 150$, highly implausible. For the observables we have used the following values: $\nu_s = 10^{19}$, $\nu_s L_s(\nu_s) = 5 \cdot 10^{45}$ erg/s, $\nu_c L_c(\nu_c) = 1.5 \cdot 10^{45}$ erg/s and the variability time and the spectral indices as in the quiescent state. The Compton peak frequency is not well determined since the spectra measured in the TeV range suffer from various uncertainties (Samuelson et al. 1998). However all the measurements give slopes steeper than 1 indicating that the peak is at lower energies. We therefore consider values between $\nu_c = 10^{25} - 10^{26}$ Hz.

In the KN regime the parameter region allowed by the peak frequency ratio (region A) has B increasing with δ [see Fig. (6)]. The luminosity ratio (region B) has almost no intersection with region A for values of δ allowed by the transparency condition. On the other hand the emitting region could be smaller than imposed by the variability time scale by a factor larger than 3. In that case region B would extend upwards defining a permitted region at $B > 1$, $\delta > 7 - 8$

However, the condition of consistency for the value of $\gamma_b \simeq 10^6$, given in the KN limit by eq. (32) (region C), is definitely outside the parameter region allowed by the other constraints, implying that the shape of the electron spectrum cannot be determined balancing radiation losses and escape, unless again the size of the region is much smaller than estimated from the observed variability. Since the flaring state lasts much longer than the cooling time, efficient continuous reacceleration processes are needed.

A comparison of the parameter space for the low and high states of Mkn 501 indicates that not only γ_b but also B increased in the flaring state.

7. Summary and Conclusions

We have extended the analytic treatment of the spectral constraints on the SSC homogeneous model for blazars initiated by GMD including KN corrections and adding the discussion of other constraints now available. The constraints can be summarized in the magnetic field-Doppler factor plane. In principle the knowledge of $\nu_{s,peak}, \nu_{c,peak}, L_{s,peak}, L_{c,peak}$ plus t_{var} allows the determination of B, δ, γ_b, R and K. The transparency condition, the time lag condition, the cooling-escape balance are further restrictions that overconstrain the model.

In practice large uncertainties on the observational quantities still exist, but at least for the best observed TeV blazar, Mrk 421, we can significantly constrain the parameter space. We find that the radiative interpretation of the lags is consistent with the spectral

constraints. Moreover, the break in the distribution is consistent with the equilibrium between the energy losses and electron escape timescale. The derived value of the the Doppler factor is moderately large ($\delta \simeq 25$), in agreement with the values found by specific spectral fits (see e.g. Ghisellini & Maraschi 1996; Mastichiadis & Kirk 1997).

We have applied the analysis also to PKS 2155-304, a well observed object in the low energy bands, detected in two occasions with EGRET in γ-rays. Assuming consistency between all the constraints (as found in the case of Mrk 421) we estimate that the peak of the Compton component should fall at about 10^{25} Hz: for higher values we do not find consistency between the spectral constraints and the time lags as measured in the 1994 observational campaign (Urry et al. 1997). We estimate the TeV flux, which could be measured by southern Cherenkov telescopes.

The last object analized is Mrk 501, a TeV emitter that has shown a dramatic flare in April 1997. For the quiescent state we can apply the classical formulation, while for the flaring state we must use the formulae in the KN limit. The absence of information about time lags prevents to completely constrain the model: however we can estimate that the value of the Doppler factor is about 10, smaller than in the other two sources. The high state is consistent with a costant Doppler factor, but impllies an increase in γ_b and in the magnetic field. The required value of γ_b is inconsistent with cooling-escape equilibrium, indicating the need of an efficient continuous reacceleration mechanism.

In conclusion the analytic approach offers a solid basis for a general discussion of the model and its applicability to specific sources. It allows to derive parameter ranges taking into account uncertainties in the "observable" quantities and a better comprehension of the interrelations between various parameters. We stress however that Table 2 has been derived applying a number of restrictive choices and hypothesis for illustrative purposes and should not be taken at face value.

Individual fits remain essential to better understand the detailed shape of the particle spectra and their origin.

Note: after the paper was accepted we learned about the detection of PKS 2155-304 by the Durham Mark 6 Cerenkov Telescope (Chadwick et al. 1998) with a flux of $F(> 0.3TeV) = 4.2 \cdot 10^{-11}$ ph cm^{-2} s^{-1}, consistent with our estimate.

A. The Klein-Nishina limit

In this Appendix we give the expression of the Compton emissivity for the electron distribution assumed in this work and we prove eq. (14) for the frequency of the Compton peak in the KN limit. All the quantities are referred to the blob reference frame.
As previously assumed, we consider a population of relativistic electrons with a double power-law distribution with indices n_1 and n_2 and break Lorentz factor γ_b:

$$N(\gamma) = \begin{cases} K_1 \gamma^{-n_1} & \text{if } \gamma < \gamma_b \\ K_2 \gamma^{-n_2} & \text{if } \gamma_b < \gamma < \gamma_{max} \end{cases} \tag{A1}$$

where $\gamma_{max} \gg \gamma_b$.
The coefficients K_1 and K_2 are related by the condition $K_1 \gamma_b^{-n_1} = K_2 \gamma_b^{-n_2}$ which gives $K_2 = K_1 \gamma_b^{n_2 - n_1}$.
The seed photons are those emitted by the synchrotron mechanism and in the blob reference frame the radiation energy density can be written as (hereafter we use the parameter $x' = h\nu'/mc^2$)

$$\epsilon(x'_0) = \begin{cases} \epsilon_0 \left(\frac{x'_0}{x'_s}\right)^{-\alpha_1} & \text{for } x'_{min} < x'_0 < x'_s \\ \epsilon_0 \left(\frac{x'_0}{x'_s}\right)^{-\alpha_2} & \text{for } x'_{max} > x'_0 > x'_s \end{cases} \tag{A2}$$

where $\alpha_i = (n_i - 1)/2$.
Using a δ-approximation (see e.g. Coppi & Blandford 1990) the Compton emissivity in the blob reference frame can be written as:

$$j(x') = \frac{\sigma_T mc^3}{8\pi h} \int_{x_1}^{x_2} N \left[\left(\frac{3x'}{4x'_0} \right)^{1/2} \right] \left(\frac{3x'}{4x'_0} \right)^{1/2} \frac{\epsilon(x'_0)}{x'_0} dx'_0 \tag{A3}$$

where the limits of the integral are analyzed in the following.
For $N(\gamma)$ and $\epsilon(x_0)$ given above we can split the integral in four similar integrals:

$$j(x') = I_{1,1} + I_{1,2} + I_{2,1} + I_{2,2} \tag{A4}$$

The first term is:

$$I_{1,1} = C(\alpha_1) K_1 \epsilon_0 \left(\frac{x'}{x'_s} \right)^{-\alpha_1} \ln \frac{x_1}{x_2} \tag{A5}$$

with $C(\alpha_1) = (4/3)^{-\alpha_1}(\sigma_T mc^3)/(8\pi h)$. The limits are:

$$x_1 = \max\left[x'_{min}, \frac{3x'}{4\gamma_b^2}\right];\ x_2 = \min\left[x'_s, \frac{3x'}{4}, \frac{3}{4x'}\right] \tag{A6}$$

The term $3/4x'$ in the upper limit express the KN suppression of the high energy emission. It originate from the step approximation of the KN cross-section, that can be rewritten as the condition that the scattering are in the Thomson regime up to:

$$\gamma x'_0 < \frac{3}{4} \tag{A7}$$

This condition, with the use of

$$x' = (4/3)\gamma^2 x'_0 \tag{A8}$$

gives:

$$x'_0 < \frac{3}{4}\frac{1}{x'} \tag{A9}$$

that is the condition used in the integrals.

The second integral is:

$$I_{1,2} = C(\alpha_1)K_1\epsilon_0 x'^{-\alpha_1} x'^{\alpha_2}_s \frac{1}{\alpha_2 - \alpha_1}\left[x_1^{\alpha_1-\alpha_2} - x_2^{\alpha_1-\alpha_2}\right] \tag{A10}$$

where:

$$x_1 = \max\left[x'_s, \frac{3x'}{4\gamma_b^2}\right];\ x_2 = \min\left[\frac{3x'}{4}, \frac{3}{4x'}\right] \tag{A11}$$

The third term can be written as:

$$I_{2,1} = C(\alpha_2)K_1\gamma_b^{2(\alpha_2-\alpha_1)}\epsilon_0 x'^{-\alpha_2} x'^{\alpha_1}_s \frac{1}{\alpha_2 - \alpha_1}\left[x_2^{\alpha_2-\alpha_1} - x_1^{\alpha_2-\alpha_1}\right] \tag{A12}$$

where, in this case $C(\alpha_2) = (4/3)^{-\alpha_2}(\sigma_T mc^3)/(8\pi h)$ and:

$$x_1 = \max\left[x'_{min}, \frac{3x'}{4\gamma_{max}^2}\right];\ x_2 = \min\left[x'_s, \frac{3x'}{4\gamma_b^2}, \frac{3}{4x'}\right] \tag{A13}$$

The last term is:

$$I_{2,2} = C(\alpha_2) K_1 \gamma_b^{2(\alpha_2-\alpha_1)} \epsilon_0 \left(\frac{x'}{x'_s}\right)^{-\alpha_2} \ln\frac{x_2}{x_1} \tag{A14}$$

with:

$$x_1 = \max\left[x'_s, \frac{3x'}{4\gamma_{max}^2}\right];\ x_2 = \min\left[x'_{max}, \frac{3x'}{4\gamma_b^2}, \frac{3}{4x'}\right] \tag{A15}$$

The Compton emissivity around the peak in the KN limit is dominated by the contribution of $I_{1,1}$ and $I_{2,1}$ (see Fig. 2 d). One can easily see that the emissivity can be written as:

$$j(x') = C(\alpha_1) K_1 \epsilon_0 \left(\frac{x'}{x'_s}\right)^{-\alpha_1} \ln\left[\gamma_b^2 \frac{1}{x'^2}\right] + C(\alpha_2) K_1 \epsilon_0 x'^{-\alpha_1} x_s'^{\alpha_1} \left(\frac{3}{4}\right)^{\alpha_2-\alpha_1} \frac{1}{\alpha_2-\alpha_1} \tag{A16}$$

¿From this expression we can find the frequency of the Compton peak, that is the maximum of the function $j(x')x'$. Taking the derivative we can write the maximum condition as:

$$\ln\left[\gamma_b^2 \frac{1}{x'^2}\right] + \frac{1}{\alpha_2-\alpha_1} - \frac{2}{1-\alpha_1} = 0 \tag{A17}$$

which gives the value of the frequency of the Compton peak:

$$x'_c = \gamma_b \exp\left[\frac{1}{\alpha_1-1} + \frac{1}{2(\alpha_2-\alpha_1)}\right] \tag{A18}$$

B. Constants used in the text

The constant $\xi(\alpha_1, \alpha_2)$ has the expression:

$$\xi(\alpha_1,\alpha_2) = 2\cdot 10^{-7} \left(\frac{h}{mc^2}\right)^{\frac{4\alpha_1-3}{1-\alpha_1}} \left[\frac{f(\alpha_1,\alpha_2)}{5.7\cdot 10^{39}}\right]^{1/(1-\alpha_1)} g(\alpha_1,\alpha_2)^{\frac{2-3\alpha_1}{1-\alpha_1}} \tag{B1}$$

In Table 3 we give the value of $\xi(\alpha_1, \alpha_2)$ for some common values of the spectral indices.

REFERENCES

Bednarek, W., and Protheroe, R.J., 1997, MNRAS, 292, 646

Buckley, J. H., et al., 1996, ApJ, 472, L9

Blandford, R.D., 1993, in Compton Gamma-Ray Observatory, ed. M. Friedlander, N. Gehrels & D.J. Macomb (New York:AIP), 533

Catanese, M., et al., 1997, ApJ, 487, L143

Celotti, A., Fabian, A.C., Rees, M.J., 1998, MNRAS, 293, 239

Coppi, P.S., Blandford, R.D., 1990, MNRAS, 245, 453

Dermer, C.D., and Schlickeiser, R., 1993, ApJ, 416, 458

Dermer, C.D., Sturner, S.J., Schlickeiser, R., 1997, ApJS, 109, 103

Dondi, L., and Ghisellini, G., 1995, MNRAS, 273, 583

Edelson, R.A., et al., 1995, ApJ, 438, 120

Gaidos, J.A., et al., 1996, Nature, 383, 319

Ghisellini, G., Celotti, A., Fossati, G., Maraschi, L., Comastri, A., 1998, MNRAS, in press

Ghisellini, G., Maraschi, L., 1996, in ASP Conf. Ser. 110, Blazar Continuum Variability, ed. H.R. Miller, J.R. Webb & J.C. Noble (San Francisco:ASP),436

Ghisellini, G., Maraschi, L., Dondi, L., (GMD), 1996, A&A Supp., 120, 503

Inoue, S., and Takahara, F., 1996, ApJ, 463,555

Macomb, D.J., et al., 1995, ApJ, 449, L99 (Erratum, 1996, ApJ, 459, L111)

Maraschi, L., Ghisellini, G., Celotti, A., 1992, ApJ, 397,L5

Mastichiadis, A., and Kirk, J.G., 1997, A&A, 320, 19

Mattox, J.R., et al., 1993, ApJ, 410,609

Pian, E., et al., 1998, ApJ, 492, L17

Sambruna, R.M., et al., 1994, ApJ, 434, 468

Samuelson, F.W., et al., 1998, ApJ, 501, L17

Schubnell, M., 1997, Proceedings of the 4th Compton Symposium, AIP Conf. Proc. 410, Editors Dermer, C.D., Strickman, M.S., Kurfess, J.D., p.1386

Sikora, M., 1997, Proceedings of the 4th Compton Symposium, AIP Conf. Proc. 410, Editors Dermer, C.D., Strickman, M.S., Kurfess, J.D., p.1386

Sikora, M., Begelman, M.C., and Rees, M.J., 1994, ApJ, 421,153

Stecker, F.W., De Jager, O.C., 1997, ApJ, 476, 712

Takahashi, T., et al., 1996, ApJ, 470, L89

Urry, M., et al., 1997, ApJ, 486, 799

Vestrand, W.T., et al., 1995, 454,L93

von Montigny, C., et al., 1995, ApJ, 440, 525

Zweerink, J.A., et al., 1997, ApJ, 490, L141

This preprint was prepared with the AAS LaTeX macros v4.0.

Figure Captions

Fig. 1.— SED of Mrk 421 in two epochs (triangles and squares, data from Macomb et al. 1995). Spectra calculated with the homogeneous SSC model with the electron energy distribution $N(\gamma) = K\gamma^{-n_1}(1+\gamma/\gamma_b)^{n_1-n_2}$ are superposed to the data: both peaks are reasonably well described by this double power-law approximation. The models are calculated with the following parameters: low state: $R = 2.7 \cdot 10^{15} cm$, $B = 0.15 G$, $K = 1.7 \cdot 10^5$, $\delta = 25$, $\gamma_b = 5.6 \cdot 10^4$, $n_1 = 2.2$, $n_2 = 4.5$; flaring state: as in the low state but $\gamma_b = 1.4 \cdot 10^5$, $K = 2.4 \cdot 10^5$. Note that in the radio band ($\nu < 10^{11}$ Hz) the emission is selfabsorbed.

Fig. 2.— Inverse Compton SSC spectra calculated using the formulae described in the Appendix (the frequency is expressed as $x' = h\nu'/mc^2$). The solid line is the total spectrum, while the other curves show the contributions of electrons and photons with different energies (see the following). The spectra are obtained for fixed synchrotron peak frequency ($\nu'_s = 10^{15} Hz$) and spectral indices ($\alpha_1 = 0.5$, $\alpha_2 = 1.5$), but for different Lorentz factors of the electrons at the break. The dotted line shows the contribution from the electrons and the photons before the break ($I_{1,1}$), the short dashed line shows the contribution from the $I_{1,2}$ branch (low energy electrons and high energy photons), the long dashed line is the contribution from $I_{2,1}$ (high energy electrons and low energy photons) and finally the dot-dashed curve is the $I_{2,2}$ spectrum (the contribution from the high energy photons and high energy electrons). In panel a) $\gamma_b = 10^3$ and the Compton peak is produced in the Thomson limit: all the contributions are present and the peak frequency is given by $\nu_c = (4/3)\gamma_b^2 \nu_s$. For higher values of γ_b [panel b)] the contribution from $I_{2,2}$ begins to be suppressed; when the peak is in the KN regime [panel c) and d)] the latter contribution vanishes, while also the contribution from $I_{1,2}$ is strongly suppressed. In the strong KN limit, only the $I_{1,1}$ and $I_{2,1}$ branches are important. Note that the spectrum after the peak in the KN limit is a power-law with the same index that the $I_{2,1}$ component, $\alpha_{KN} = 2\alpha_2 - \alpha_1$

Fig. 3.— Constraints on the parameter space for Mrk 421. Region A represents the peak frequency constraint. The region takes into account an uncertainty of a factor 3 in the position of the Compton peak, the upper line is calculated for $\nu_c = 2 \cdot 10^{25}$ Hz, the lower line for $\nu_c = 1.8 \cdot 10^{26}$ Hz and the intermediate line for $\nu_c = 6 \cdot 10^{25}$ Hz. Region B is obtained from the peak luminosity constraint and takes into account an uncertainty of a factor 3 in the dimension of the region (the upper line is calculated for $t'_{var} = 1/3 t_{var}$). The region C is obtained from the equilibrium of cooling and escape for electrons with Lorentz factor γ_b; the region is plotted taking into account an uncertainty of a factor 3 in the value of t_{var} and

in the value of β_{esc} (1-1/3). The thick line l is obtained from the observed time lag between variations in different X-ray band. The vertical line shows the lower limit on δ given by the transparency condition. The plot shows that consistency of all the constraints is achieved for $\delta \simeq 25$ and $B \simeq 0.2$

Fig. 4.— Parameter space for PKS 2155-304. Lines and regions are labelled as in Fig. 3. Region A takes into account an uncertainty of a factor 3 in the Compton peak frequency ($2.5 \cdot 10^{24}$–$2.5 \cdot 10^{25}$).

Fig. 5.— Parameter space for Mrk 501 (low state). For this object we do not have information about delays in the variability and therefore in the diagram we cannot plot the line l.

Fig. 6.— Parameter space for Mrk 501 (high state). In this case we have used the formulae for the KN limit and region A has a positive slope. Note that the break energy–balance condition between energy losses and escape (region C) is not consistent with the other constraints.

Table 1. Input observational quantities

	Mrk 421	PKS 2155-304	Mrk 501 (l.s.)	Mrk 501 (h.s.)
ν_s (Hz)	$3 \cdot 10^{16}$	10^{16}	10^{16}	10^{19}
ν_c (Hz)	$2 \cdot 10^{25} - 2 \cdot 10^{26}$	$2.5 \cdot 10^{24} - 2.5 \cdot 10^{25}$	$3 \cdot 10^{24} - 3 \cdot 10^{25}$	$10^{25} - 10^{26}$
$\nu_s L_s(\nu_s)$	$4.7 \cdot 10^{44}$	$1.5 \cdot 10^{46}$	10^{44}	$5 \cdot 10^{45}$
$\nu_c L_c(\nu_c)$	$6.3 \cdot 10^{44}$	$1.5 \cdot 10^{46}$	$5 \cdot 10^{43}$	$1.5 \cdot 10^{45}$
t_{var} (h)	1	5.5	10	10
$\tau^a_{obs}(s)$	4200	4700	-	-

[a]lag between photons of 5 keV and 0.75 keV

Table 2. Physical parameters estimated from the present analysis

	Mrk 421	PKS 2155-304	Mrk 501 (l.s.)	Mrk 501 (h.s.)
δ	$22-35$	$24-38$	$8-20$	7
B (G)	$0.3-0.2$	$0.3-0.2$	$0.5-0.1$	1
γ_b^a	$4-3$	$2-1.8$	$3-4$	60
R^b	$3-1$	$15-7$	$9-7$	2.5

[a]in units of 10^4.

[b]in units of 10^{15} cm.

Table 3. Values of $\xi(\alpha_1, \alpha_2)$ for some values of the spectral indices

α_1	α_2	$\xi(\alpha_1, \alpha_2)$
0.5	1.25	$9.13 \cdot 10^{-46}$
0.5	1.75	$2.17 \cdot 10^{-46}$
0.75	1.25	$1.54 \cdot 10^{-161}$
0.75	1.75	$1.1 \cdot 10^{-165}$

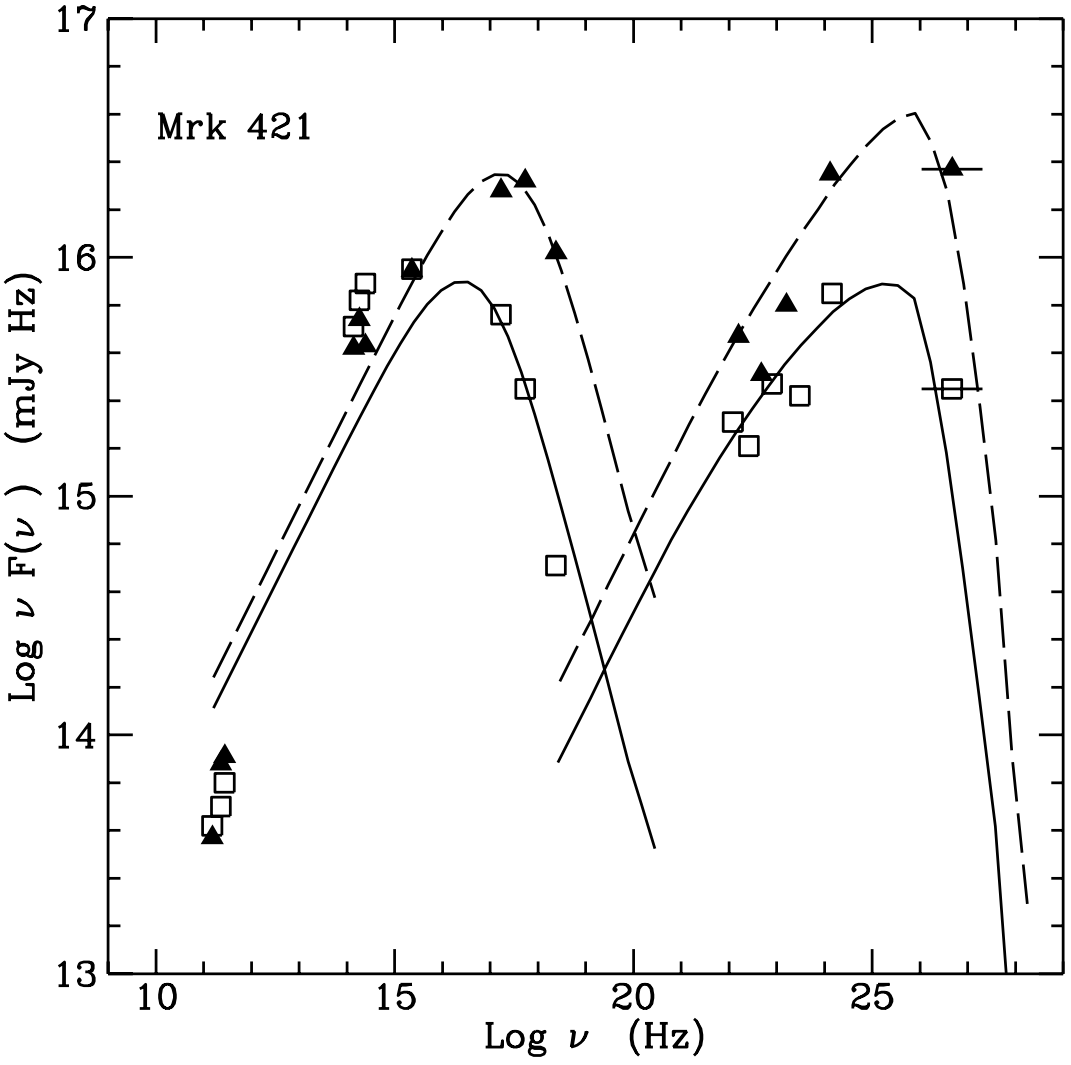
Mrk 421
Log ν F(ν) (mJy Hz)
Log ν (Hz)
17
16
15
14
13
10
15
20
25

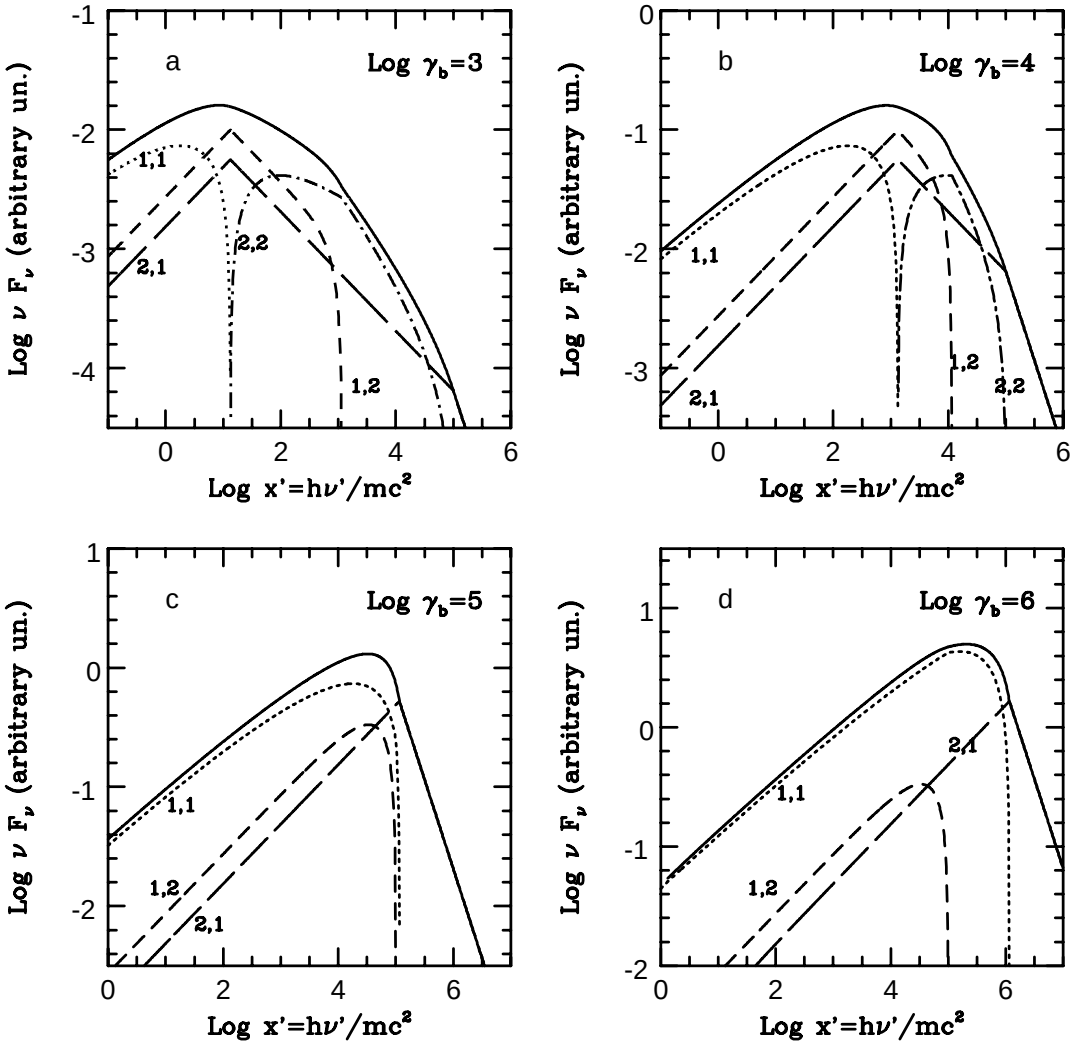
a
Log γ_b=3
1,1
2,1
2,2
1,2
b
Log γ_b=4
1,1
2,1
1,2
2,2
c
Log γ_b=5
1,1
1,2
2,1
d
Log γ_b=6
1,1
2,1
1,2
Log ν F_ν (arbitrary un.)
Log x'=hν'/mc^2

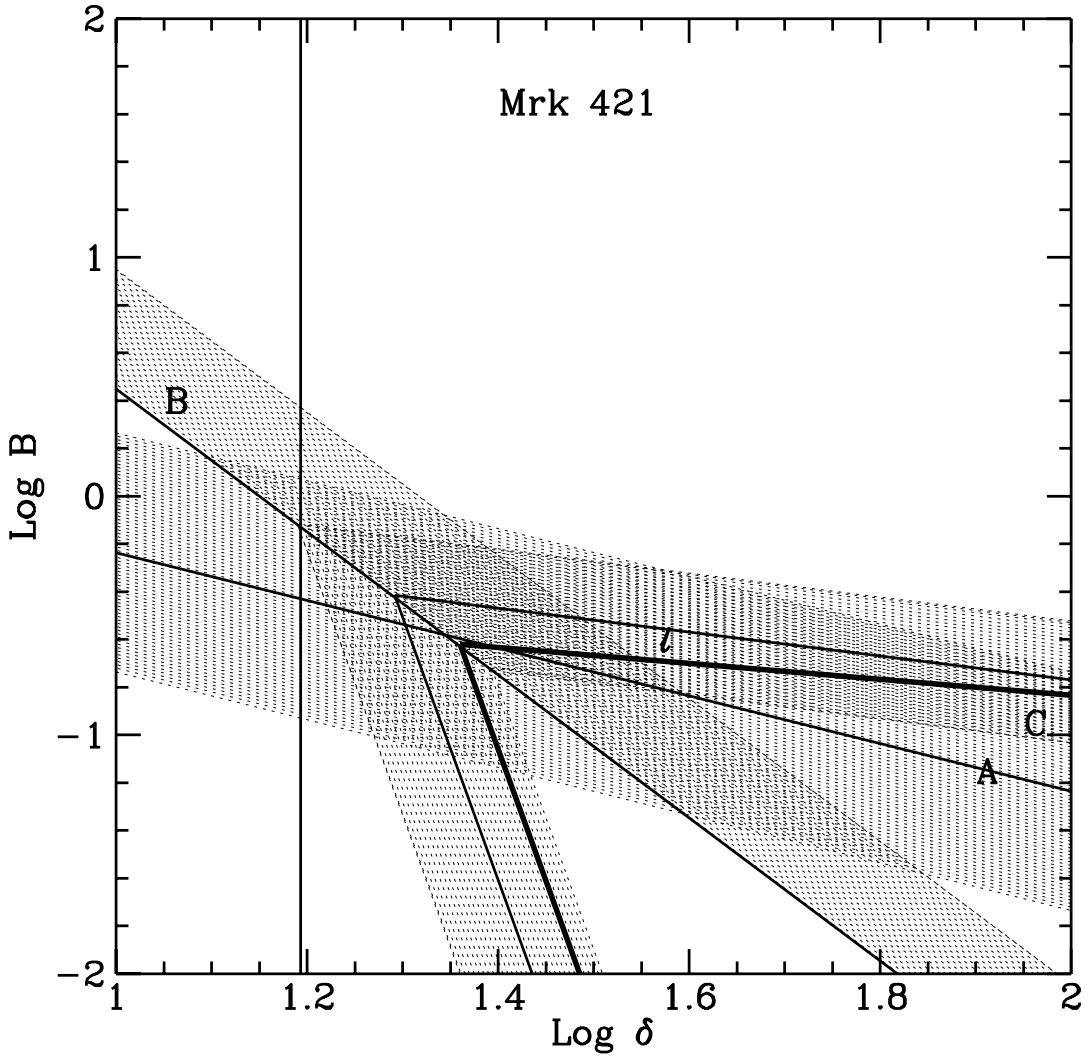
Mrk 421
B
A
C
Log B
Log δ
2
1
0
−1
−2
1
1.2
1.4
1.6
1.8
2

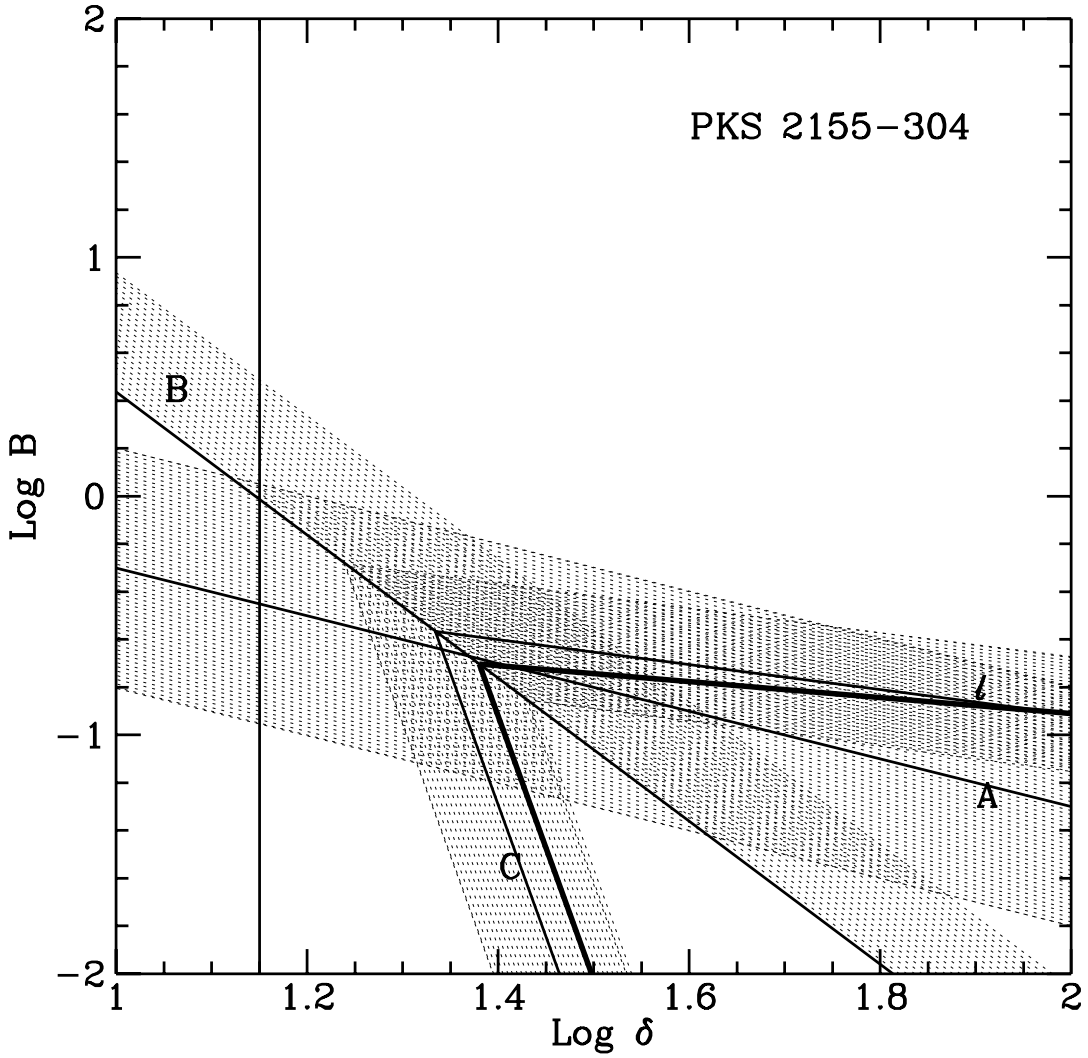
PKS 2155−304
B
A
C
b
Log B
Log δ
2
1
0
−1
−2
1
1.2
1.4
1.6
1.8
2

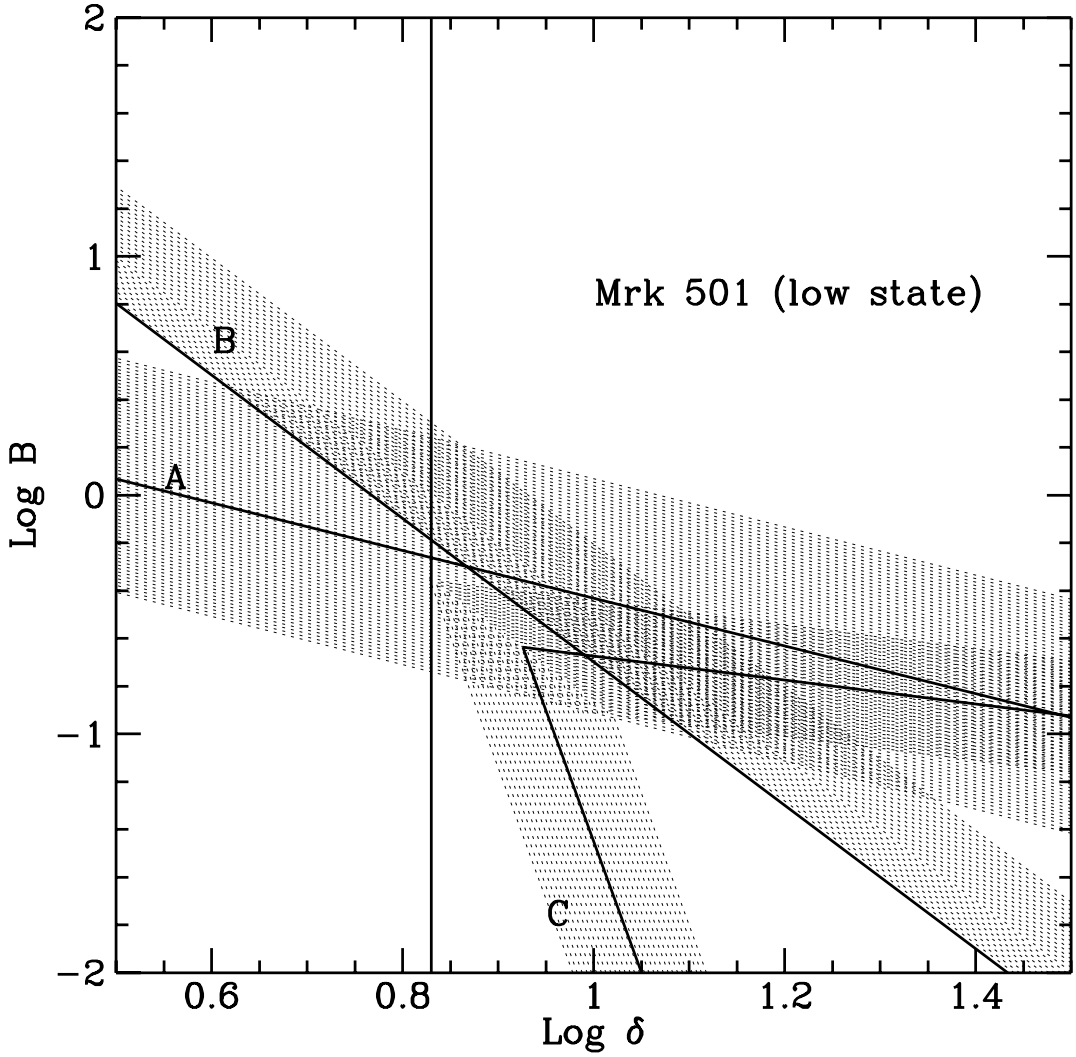
Mrk 501 (low state)
B
A
C
Log B
Log δ
2
1
0
−1
−2
0.6
0.8
1
1.2
1.4

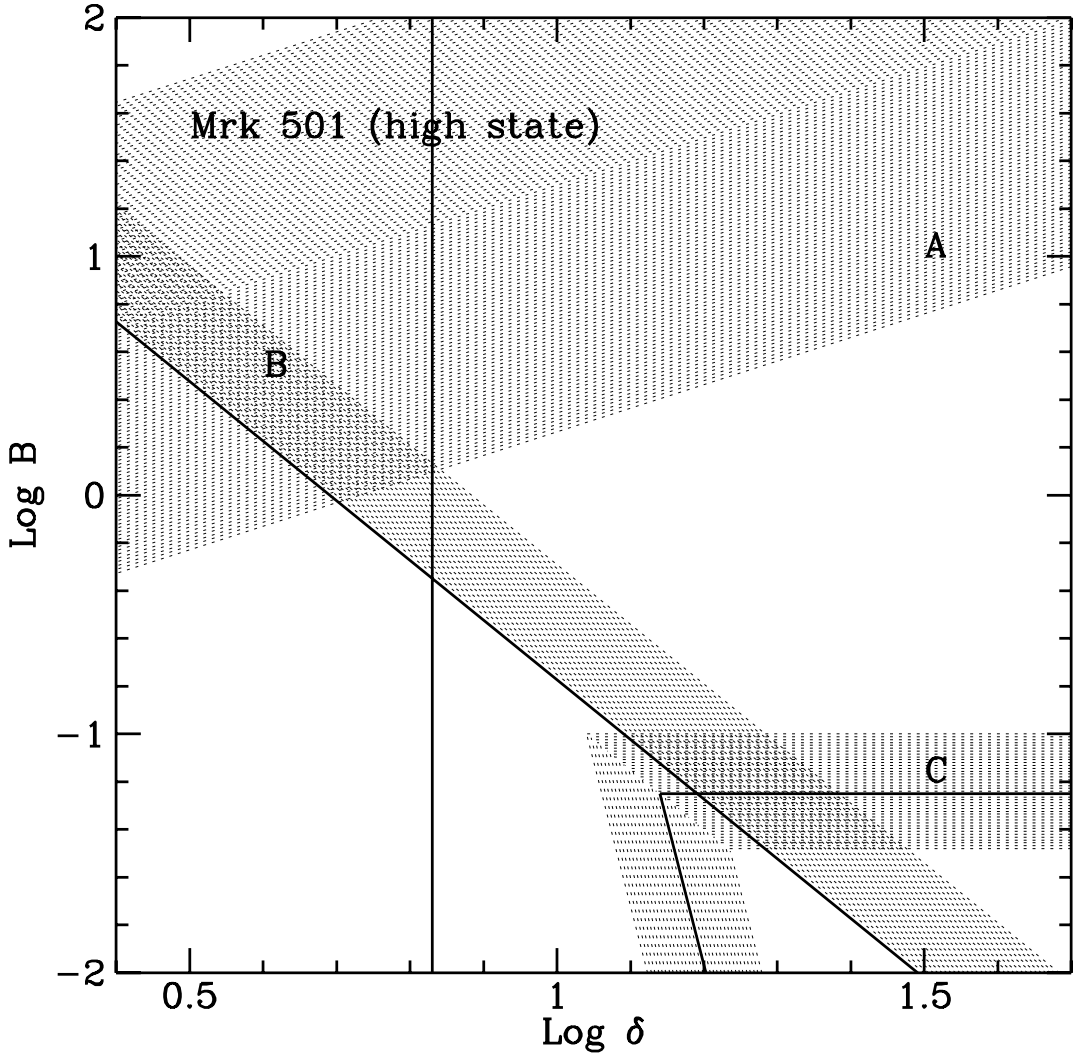
Mrk 501 (high state)
A
B
C
Log B
Log δ
2
1
0
−1
−2
0.5
1
1.5